Accepted version of paper submitted to Journal of Optimization Theory and Applications. DOI from Springer is not yet available.

Energy Optimal Speed Profiles for a Differential Drive Mobile Robot with Payload

Mauricio F. Jaramillo-Morales[1], Sedat Dogru[2], Lino Marques[2]

[1]Departamento de Electrónica y Automatización,
Universidad Autónoma de Manizales
Manizales - Colombia, 38-122, Cra. 21 #38-52,
Manizales, Caldas, Colombia
mfjaramillo@autonoma.edu.co

[2]Institute of Systems and Robotics,
Department of Electrical and Computer Engineering,
University of Coimbra, 3030-290 Coimbra, Portugal
{sedat, lino}@isr.uc.pt

Abstract

Mobile robots are being used more widely in various environments, such as households, hospitals, agriculture, and industry. In these spaces, many times the robots are required to cover long distances, at times carrying heavy payloads, resulting in large energy consumption. In order to reduce the energy consumption, this paper presents a set of novel optimal speed profiles for two wheel differential drive robots. The profiles are derived using Hamiltonian formalism, resulting in closed-form speed profiles for both straight and rotational motions. The derivation used a power model that explicitly considers robot and motor dynamic parameters as well as external payload. Energy consumption of a commercial two wheel differential drive robot was experimentally evaluated using various trapezoidal and the proposed optimum speed profiles, showing significant energy savings using the new speed profiles. The paper also presents an analysis on variations of trajectory times and maximum speeds with varying payloads.

1 Introduction

Wheeled mobile robots (WMR) have been successfully adopted for various applications over time, and new application areas are emerging everyday. Energy efficiency of these platforms is an important topic, and it is motivated by the need to save on energy bills, consume less energy to be environmentally friendly, and also the fact that they have limited on board energy sources, which can restrict their operating times. Energy consumption of a WMR depends on several parameters, such as surface friction [4, 20], regularity and slope of the surfaces [9, 11], losses in onboard electronic

devices [5, 13, 21, 27], accelerations of the robot, and overall weight, which can change significantly for load carrying robots [14, 21].

Energy consumption of a WMR can be reduced in several ways, the most trivial being traveling along the shortest feasible path connecting the start and end points, taking into account robot headings. In the case of car-like robots, the initial and final headings, as well as the minimum turning radius, impose additional constraints, resulting in shortest paths that contain curves such as Dubins curves [6], or Reeds-Shepp curves [22], rather than just straight lines. The first type of curves allows only forward motion, and the second type allows forward and backward motion. These paths, however, do not have a continuous curvature, requiring a full stop of the car like platform to switch between the different segments of the paths. Fraichard et al. [7] introduced continuity of the curvature as a constraint, ending in longer paths. Later, Chitsaz et al. [2], following the footsteps of Dubins, classified trajectories of differential drive robots (DDR), optimizing the total amount of wheel rotations. They also found out the equivalence of time minimum Reeds and Shepp paths and minimum wheel rotation DDR paths. Furtuna and Balkcom [8] pushed forward this line of research and presented curves for the fastest trajectories between two robot poses, assuming a generic robot that is defined by a 2D pose and corresponding speeds, irrespective of driving mechanism.

The trajectory, which defines the accelerations and speeds of the robot along the path, also plays an important role in the overall energy consumption. This consumption can be significantly reduced by optimizing the trajectory for each path. Kim and Kim [16] optimized the power consumption of a DDR using only the motor model, not taking into account the dynamic parameters of the robot. They compared the results with both a path minimizing only armature losses of the motor, and a trajectory using standard trapezoidal speed profiles. Tokekar et al. [26] studied a car-like robot, using a polynomial model built from a model of a brushed DC motor. They also presented a calibration procedure to find the constant coefficients of the polynomial, and compared the optimum profile with trapezoidal profiles. Nevertheless, the approach is not flexible since calibration should be done whenever the payload or surface change. More complex power models have been used for skid-steered platforms [4, 12, 20]. These models take into account dynamic forces, friction losses, and the characteristics of the path in power estimation. Once a power estimation model is obtained, optimization procedures can be applied to calculate the optimal velocities that minimize the robot's energy for different paths. Morales et al. [20] presented a power estimation model for a skid-steered mobile robot based on friction of the wheels on natural terrains. The results confirm that the energy consumption depends on the total turned angle. Dogru and Marques [4] presented a similar approach, taking into account varying payloads. The simple or more complex power models have also been used in high level path planners. Gupta et al. [12] used the Lagrange formulation to model the power of a skid-steer robot, complementing it with A* path optimization to improve the energy consumption for different speeds, surfaces, and payloads. Liu et al. [17] used an energy function considering kinetic energy, surface friction and sensor consumption of DDR. Later, this energy function is used as part of the cost function in A* search to find an optimal path in cluttered space. Sathiya and Chinnadurai [23] formulated a multi-objective minimization problem to minimize the mission time and the overall ac-

tuator effort using a genetic algorithm. They took into account only the kinetic energy of the platform and the kinematic constraints to derive the torque equations. Serralheiro et al. [24] studied time-energy minimization for WMRs using a simplified robot dynamics model. Mei et al. [19] studied coverage of space using different path and speed profiles for an omni-WMR, utilizing a polynomial of degree six as the power model. Perez et al. [25] studied control of omni-WMR subject to minimization of tracking error and energy consumption, approximating the second with the square of the torque.

Morales et al. [15] take a different road by optimizing the speed profile along straight paths, which may be used as motion primitives of a general trajectory. This work extends [15] by studying the optimization along circular paths. The speed profiles are given in closed form, and they are derived using the Hamiltonian from optimal control theory [18], and a power model recently proposed by the authors [14]. The model explicitly contains internal parameters belonging to the motor and the robot, and external parameters, which are friction and payload. The internal parameters can be obtained from motor and robot datasheets, and the friction has to be estimated experimentally. To the best of the authors' knowledge, this is the first study that takes both robot and motor parameters explicitly into account and the first study that presents a closed form solution to the minimum energy trajectory. Using the proposed approach, variations in payload can easily be taken into account to generate the optimal speed profiles. Finally, the optimal profiles are validated experimentally with a Nomad Super Scout robot, showing considerable energy savings along straight and circular paths.

The next section summarizes the power estimation model, given by the combination of robot and motor dynamic models [15]. Then, a mathematical optimization procedure to obtain optimal speed profiles using the Hamiltonian formalism is provided. The third section describes the experimental setup and the robot. Section IV presents the experimental results and compares the optimal speed profiles with trapezoidal speed profiles for straight and circular paths. It also presents an analysis on variations of trajectory times and maximum speeds with varying payloads. Finally, Section V concludes this work.

2 Development of the Optimal Velocity Profile

This section develops the mathematical procedure to calculate wheels' optimal speed profiles that minimize the energy consumption of a differential drive mobile robot for straight and curved paths. The mathematical model considers the total mass of the robot, including the payload. The first subsection shows the methodology to find the power model of the robot that is used to build the Hamiltonian function to optimize. As a result, a closed-form mathematical solution is obtained. The parameters of the mathematical models are presented in Table 1.

2.1 Power Model

The proposed WMR power model combines the classical dynamic model of a WMR robot and the dynamic model of an electric motor. The development of these models

Table 1: Symbols used in this work

Symbol	Description
x and y	Coordinates of the geometric center of the robot (P_o in Figure 1) in a fixed reference coordinate frame X - Y
ϕ	Heading angle of the mobile robot measured from the X-axis
$\dot{\phi}$	Angular velocity of the robot $c(\dot{\theta}_1 - \dot{\theta}_2)$
$\ddot{\phi}$	Angular acceleration of the robot $c(\ddot{\theta}_1 - \ddot{\theta}_2)$
v	Linear velocity of the robot
θ_i	Angular position of the wheels
$\dot{\theta}_i$	Angular velocity of the wheels
$\ddot{\theta}_i$	Angular acceleration of the wheels
Γ	Radius of curvature of the robot path
a	Ratio of wheel speeds ($\dot{\theta}_2/\dot{\theta}_1$)
A	Motion constraints matrix
τ_j	Load torques applied to the wheels (the part due to acceleration)
T_a	Load torque applied to the motor (the part due to acceleration)
l	Half the distance between the wheels
d	The distance between the center of mass and the geometric center of the robot
r	Radius of the driving wheels
c	Constant that is equal to $\frac{r}{2l}$
m_c	Mass of the mobile robot without the driving wheels and the rotors of the motors, plus payload
m_w	Mass of each driving wheel plus the rotor of its motor
m	Total mass, m_c + $2m_w$
ν	Viscous friction coefficient
I_c	Moment of inertia of the mobile robot and the payload without the driving wheels and the rotors of the motors about a vertical axis passing through the intersection of the axis of symmetry with the driving wheel axis. The robot is assumed to be a solid cylinder.
I_w	Moment of inertia of each driving wheel and the motor rotor about the wheel axis. The wheel is assumed to be a thin circular loop.
I_m	Moment of inertia of each driving wheel and the motor rotor about wheel diameter
I_s	Equivalent motor moment of inertia
I	Equivalent inertia given by $I = I_c + 2m_w l^2 + 2I_m$
R and L	Armature resistance and inductance
K_t and K_v	Motor friction torque and voltage constants
n	Gear ratio of the motor
T_m	Torque due to surface friction and friction in the drive-train
$\mathbf{V} = [V_1\ V_2]^T$	Armature voltages of the motors of the robot
$\mathbf{i} = [i_1\ i_2]^T$	Currents of the motors of the robot
$\mathbf{P} = [P_1\ P_2]^T$	Power consumed by the motors of the robot
$\lambda = [\lambda_1\ \lambda_2]^T$	Lagrange multipliers
$q = [x\ y\ \theta_1\ \theta_2]^T$	Generalized coordinate

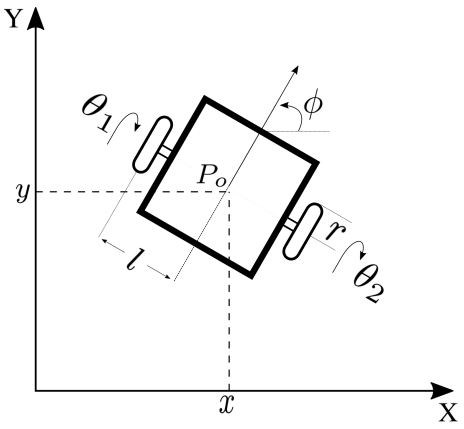

Figure 1: Schematic of a two wheel differential drive mobile robot.

uses a state-space transformation to express the motor voltages as a function of the parameters of the robot and the motor. Finally, the power model is calculated by the multiplication of the voltage and the current of the dynamic motor model. This model was already developed and extensively tested in a prior work [14], but it is summarized here for easy reference.

2.1.1 Dynamic Model of a Two-Wheel Differential Drive Robot

The dynamic model of a differential drive mobile robot that is represented by nonlinear differential equations can be found with the Lagrange formulation, which depends on the kinetic energy K, using

$$\frac{d}{dt}\left(\frac{\partial K}{\partial \dot{q}_i}\right) - \left(\frac{\partial K}{\partial q_i}\right) = \tau_j - a_{1i}\lambda_1 - a_{2i}\lambda_2 \,. \tag{1}$$

Here, i= 1, ..., 4 is the index for the generalized coordinates $q = [q_1\ q_2\ q_3\ q_4]^T$ = $[x\ y\ \theta_1\ \theta_2]^T$, and $[a_{1i}\ a_{2i}]^T$ are the elements of the motion constraint matrix. Moreover, j = 1,2 is the index for τ_j the load torque of the wheels related with the angular velocity of the wheels $\dot{\theta_1}$ and $\dot{\theta_2}$.

The total kinetic energy of the mobile robot is given by

$$\begin{aligned} K = &\frac{1}{2}m(\dot{x}^2 + \dot{y}^2) + m_c c d(\dot{\theta_1} - \dot{\theta_2})(\dot{y}\cos\phi - \dot{x}\sin\phi) \\ &+ \frac{1}{2}I_w({\dot{\theta_1}}^2 + {\dot{\theta_2}}^2) + \frac{1}{2}Ic^2(\dot{\theta_1} - \dot{\theta_2})^2 \,, \end{aligned} \tag{2}$$

where $I = I_c + 2m_w l^2 + 2I_m$. This total kinetic energy (equation 2) can be rewritten as

$$K = K_T + K_r + K_m + K_w \,, \tag{3}$$

where K_T is the kinetic energy of translation, K_r is the kinetic energy of rotation, K_m is the mobile inertia moment without wheels, and K_w is the wheel inertia moment.

The parameters a_{ij} of the dynamic model (1), are calculated considering the two motion constraints of the differential drive mobile robot (Fig. 1). These restrictions can be stated as follows:

- The mobile robot can not move in a lateral direction, implying

$$\dot{x}\sin\phi - \dot{y}\cos\phi = 0\,. \tag{4}$$

- The two driving wheels of the mobile robot roll and do not slip, implying

$$\dot{x}\cos\phi + \dot{y}\sin\phi + l\dot{\phi} = r\dot{\theta_1}\,, \tag{5}$$

$$\dot{x}\cos\phi + \dot{y}\sin\phi - l\dot{\phi} = r\dot{\theta_2}\,. \tag{6}$$

Here (x, y) are the coordinates of point P_o in the fixed reference coordinated frame $X - Y$, ϕ is the heading angle of the mobile robot measured from the X-axis, and θ_1, θ_2 are the angular positions of the left and right driving wheels.

Adding equations (5) and (6), equation (7) is obtained as

$$\dot{x}\cos\phi + \dot{y}\sin\phi = \frac{r}{2}(\dot{\theta_1} + \dot{\theta_2})\,. \tag{7}$$

Equations (4) and (7) can be expressed in matrix form as

$$\begin{bmatrix} a_{11} & a_{12} & a_{13} & a_{14} \\ a_{21} & a_{22} & a_{23} & a_{24} \end{bmatrix} \begin{bmatrix} \dot{x} \\ \dot{y} \\ \dot{\theta_1} \\ \dot{\theta_2} \end{bmatrix} = 0\,. \tag{8}$$

The components of the motion constraints matrix are given by

$$\begin{bmatrix} a_{11} & a_{12} & a_{13} & a_{14} \\ a_{21} & a_{22} & a_{23} & a_{24} \end{bmatrix} = \begin{bmatrix} -\sin\phi & \cos\phi & 0 & 0 \\ -\cos\phi & -\sin\phi & \frac{r}{2} & \frac{r}{2} \end{bmatrix}\,. \tag{9}$$

Matrix equation (8) can be written as

$$A(q)\dot{q} = 0\,. \tag{10}$$

Once the derivatives of the Lagrange equation are calculated, the nonlinear dynamic system of equations that represents the dynamic model of the mobile robot is obtained as

$$\begin{aligned} \lambda_1\sin\phi + \lambda_2\cos\phi &= m\ddot{x} - m_c d(\ddot{\phi}\sin\phi + \dot{\phi}^2\cos\phi)\,, \\ -\lambda_1\cos\phi + \lambda_2\sin\phi &= m\ddot{y} + m_c d(\ddot{\phi}\cos\phi - \dot{\phi}^2\sin\phi)\,, \\ \tau_1 - cl\lambda_2 &= m_c cd(\ddot{y}\cos\phi - \ddot{x}\sin\phi) + \\ &\quad (Ic^2 + I_w)\ddot{\theta_1} - Ic^2\ddot{\theta_2}\,, \\ \tau_2 - cl\lambda_2 &= -m_c cd(\ddot{y}\cos\phi - \ddot{x}\sin\phi) - \\ &\quad Ic^2\ddot{\theta_1} + (Ic^2 + I_w)\ddot{\theta_2}\,. \end{aligned} \tag{11}$$

This equation system is based on the kinematic model of the robot represented Fig. 1, and the Lagrange formulation [10, 28, 29]. The load torques applied to the wheels (τ_1, τ_2) are considered in the third and fourth equations of (11) because these equations are related directly to the angular velocity of the wheels.

2.1.2 Dynamic Model of a Motor

The WMR studied in this work is a two-wheel symmetric structure. Therefore, it can be assumed that the motors in both wheels have the same dynamic parameters. In that case, the dynamic model of the motors is represented by the following differential equation system:

$$\begin{aligned} L\dot{i} + Ri + K_v n\dot{\theta} &= V\,, \\ K_t n i - I_s\ddot{\theta} - \nu\dot{\theta} &= T_a + T_m\,. \end{aligned} \tag{12}$$

The first equation in (12) is the voltage equation of a DC motor, and the second equation is the current equation that relates the current to the torque due to frictions of the surface and of the drive train of the motor (T_m) and to the torque due to accelerations (T_a). The inductance of the armature circuits may be ignored because the electrical response is, in general, much faster than the mechanical response. Therefore, the first expression of equation (12) yields

$$i = \frac{V - K_v n\dot{\theta}}{R}\,. \tag{13}$$

Then, the variable i is replaced in the second expression of equation (12), and the torque due to acceleration (T_a) is obtained as

$$T_a = \frac{K_t n}{R}V - I_s\ddot{\theta} - \left(\frac{K_t K_v n^2}{R} + \nu\right)\dot{\theta} - T_m\,. \tag{14}$$

2.1.3 Combined Dynamic Model

The robot's power model combines the dynamic model of the WMR and the dynamic motor model. Once both models are merged, replacing the torque due to accelerations (equation (14)) in equation (11), considering $\tau_1 = \tau_2 = T_a$, because of the wheels' and motors' symmetries, the combined dynamic model can be ordered and expressed in matrix form as

$$M(q)\ddot{q} + F\dot{q} + C(q,\dot{q}) = T\mathbf{V} - A^T(q)\lambda\,, \tag{15}$$

where

$$M(q) = \begin{bmatrix} m & 0 & -\alpha_1 & \alpha_1 \\ 0 & m & \alpha_2 & -\alpha_2 \\ -\alpha_1 & \alpha_2 & Ic^2 + I_w + I_s & -Ic^2 \\ \alpha_1 & -\alpha_2 & -Ic^2 & Ic^2 + I_w + I_s \end{bmatrix},$$

$$\alpha_1 = m_c cd\sin\phi\,,$$

$$\alpha_2 = m_c cd\cos\phi\,,$$

$$F = \begin{bmatrix} 0 & 0 & 0 & 0 \\ 0 & 0 & 0 & 0 \\ 0 & 0 & \dfrac{K_t K_v n^2}{R} + \nu & 0 \\ 0 & 0 & 0 & \dfrac{K_t K_v n^2}{R} + \nu \end{bmatrix},$$

$$C(q,\dot{q}) = \begin{bmatrix} -m_c d\dot{\phi}^2 \cos\phi \\ -m_c d\dot{\phi}^2 \sin\phi \\ T_m \\ T_m \end{bmatrix}, \qquad T = \begin{bmatrix} 0 & 0 \\ 0 & 0 \\ \dfrac{K_t n}{R} & 0 \\ 0 & \dfrac{K_t n}{R} \end{bmatrix},$$

$$A(q) = \begin{bmatrix} -\sin\phi & \cos\phi & 0 & 0 \\ -\cos\phi & -\sin\phi & cl & cl \end{bmatrix}. \tag{16}$$

In order to reduce the order and simplify the combined differential system, a state space realization is applied. In that case, the following null space matrix $S(q)$ of the matrix $A(q)$ is used:

$$S(q) = \begin{bmatrix} cl\cos(\phi) & cl\cos(\phi) \\ cl\sin(\phi) & cl\sin(\phi) \\ 1 & 0 \\ 0 & 1 \end{bmatrix}. \tag{17}$$

New variables are introduced using the null space matrix, then $S^T(q)A^T(q)\eta = 0$, where $\eta = [\dot{\theta}_1 \;\; \dot{\theta}_2]^T$, increasing the state space variables to $\mathbf{x} = [x \;\; y \;\; \theta_1 \;\; \theta_2 \;\; \dot{\theta}_1 \;\; \dot{\theta}_2]^T$.

Now, multiplying both sides of equation (15) by $S^T(q)$ and using the result $S^T(q)A^T(q) = 0$, it can be said that

$$S^T(q)M(q)\ddot{q} + S^T(q)F\dot{q} + S^T(q)C(q,\dot{q}) = S^T(q)TV - S^T(q)A^T(q)\lambda\,. \tag{18}$$

The equation $\dot{q} = S(q)\eta$ can be derived again, and the variable $\ddot{q}$ is obtained as

$$\ddot{q} = S(q)\dot{\eta} + \dot{S}(q)\eta\,. \tag{19}$$

Then, both variables $\dot{q}$ and $\ddot{q}$ are replaced in equation (18) giving

$$S^T M(S\dot{\eta} + \dot{S}\eta) + S^T F(S\eta) + S^T C = S^T TV\,. \tag{20}$$

Finally, the voltage expression can be isolated from equation (20), giving

$$\mathbf{V} = (S^T T)^{-1}(S^T MS\dot{\eta} + S^T M\dot{S}\eta + S^T FS\eta + S^T C)\,. \tag{21}$$

The voltage variable from equation (21) is replaced in equation system (12) and then the current is calculated. Finally, the voltage and current variables are multiplied, which leads to the following power estimation model

$$\boldsymbol{P(t)} = \mathbf{V}^T(t)\;\mathbf{i}(t)\,. \tag{22}$$

Here $\boldsymbol{P(t)} = [P_1(t) \;\; P_2(t)]^T$ represents the power of each wheel. Then, the total power estimation is the sum $P(t) = P_1(t) + P_2(t)$, which depends on speed and acceleration of both wheels.

2.1.4 Power Model of a WMR Along a Straight Path

The power model (equation (22)) can be simplified along straight paths, taking into account the kinematic characteristics. When the robot follows a straight path, the angular speeds and accelerations of both wheels must be the same. ($\dot{\theta}_2 = \dot{\theta}_1$, $\ddot{\theta}_2 = \ddot{\theta}_1$). Taking the start of straight motion as the origin for the angular positions of the wheels, they are also expected to be the same ($\theta_2 = \theta_1$). Similarly, the angular velocity of the robot is zero ($\dot{\phi} = 0$), and the orientation of the robot can be taken to be zero ($\phi = 0$) for power estimation purposes. Hence, doing the corresponding replacements in the power model and using an equivalent inertia I_e given by

$$I_e = 2I_s + m_c r^2 + 4m_w r^2 \tag{23}$$

the following expression is obtained for the power consumption of a DDR along a straight path.

$$P_s = \frac{R}{2{K_t}^2 n^2}\left(2T_m + I_e\ddot{\theta}_1 + 2\nu\dot{\theta}_1\right)^2 + \frac{K_v}{K_t}\left(2T_m + I_e\ddot{\theta}_1 + 2\nu\dot{\theta}_1\right)\dot{\theta}_1\,. \tag{24}$$

2.1.5 Power Model of a WMR Along a Curved Path

A circular path can be generated using the following equations:

$$\begin{aligned} x &= \Gamma\sin\phi\,,\\ y &= \Gamma\cos\phi\,. \end{aligned} \tag{25}$$

where x and y represent the coordinate position of the robot along the circular path, and Γ is its radius. Then taking the derivative of both equations, we get

$$\begin{aligned} \dot{x} &= \Gamma\,\dot{\phi}\cos\phi\,,\\ \dot{y} &= -\Gamma\,\dot{\phi}\sin\phi\,. \end{aligned} \tag{26}$$

The linear and angular velocities of a differential drive mobile robot are given by

$$\begin{aligned} \dot{x} &= \frac{r(\dot{\theta}_1 + \dot{\theta}_2)}{2}\cos\phi\,,\\ \dot{y} &= \frac{r(\dot{\theta}_1 + \dot{\theta}_2)}{2}\sin\phi\,,\\ \dot{\phi} &= \frac{r(\dot{\theta}_1 - \dot{\theta}_2)}{2l}\,. \end{aligned} \tag{27}$$

Replacing $\dot{x}$ of (26) in (27), the following relationship between the wheels is reached:

$$\Gamma\dot{\phi} = \frac{r(\dot{\theta}_1 + \dot{\theta}_2)}{2}\,. \tag{28}$$

Then, replacing the variable $\dot{\phi}$ of equation (27) in equation (28), and isolating the variable $\dot{\theta}_2$, the following relationship is obtained:

$$\dot{\theta}_2 = \dot{\theta}_1\left(\frac{\Gamma - l}{\Gamma + l}\right)\,. \tag{29}$$

Isolating $\dot{\theta}_2$ avoids the divide by zero possibility. Hence, assuming that the starting angular positions of the wheels are zero for power estimation purposes, the following relationships can be assumed to hold:

$$\begin{aligned} \theta_2 &= a\theta_1 \,, \\ \dot{\theta_2} &= a\dot{\theta_1} \,, \\ \ddot{\theta_2} &= a\ddot{\theta_1} \,, \end{aligned} \tag{30}$$

where

$$a = \frac{\Gamma - l}{\Gamma + l} \,. \tag{31}$$

Hence using (30) and introducing a new constant I_p to stand for variation in the perceived inertia of the motors, with I_p given as

$$I_p = (1-a)\left(\frac{m_w r^4}{2l^2} - \frac{m_c r^2}{4}\right) \,, \tag{32}$$

the following equations are obtained for the power consumption of each wheel

$$\begin{aligned} P_1 =& \frac{R}{4{K_t}^2 n^2}\left(2T_m + (I_e + I_p)\,\ddot{\theta}_1 + 2\nu\dot{\theta}_1\right)^2 \\ &+ \frac{K_v}{2K_t}\left(2T_m + (I_e + I_p)\,\ddot{\theta}_1 + 2\nu\dot{\theta}_1\right)\dot{\theta}_1 \,, \end{aligned} \tag{33}$$

$$\begin{aligned} P_2 =& \frac{R}{4{K_t}^2 n^2}\left(2T_m \operatorname{sgn} a + (aI_e - I_p)\,\ddot{\theta}_1 + 2a\nu\dot{\theta}_1\right)^2 \\ &+ \frac{K_v}{2K_t} a\left(2T_m \operatorname{sgn} a + (aI_e - I_p)\,\ddot{\theta}_1 + 2a\nu\dot{\theta}_1\right)\dot{\theta}_1 \,. \end{aligned} \tag{34}$$

Above, sgn stands for the signum function, and makes sure that the friction torque T_m is always opposing the motion of the second wheel, even when it starts to rotate along the opposite direction of the first wheel. The fact that the outer wheels consume more power is apparent from the above equations ($P_1 > P_2$ for $0 < a < 1$). Note that, for $a = 1$, these equations are equivalent to the power equations of straight motion. Both I_p and I_e depend on the moment of inertia of the robot body and the wheels. However, these objects are generally not uniform, making exact modeling of the corresponding moments of inertia infeasible. Nonetheless, it was experimentally observed that approximate models were sufficient to produce paths that are more energy efficient than the trapezoidal speed profiles.

2.2 Hamiltonian Function Optimization

This section presents a closed-form mathematical expression for the optimal speed of the mobile robot that minimizes power consumption. First, the problem statement that delimits the initial and final conditions is shown. Then, the optimal speed profile is calculated using the Hamiltonian function and the necessary optimal conditions. Finally, the final time is obtained with the transversality condition.

2.2.1 Problem Statement

The power models P_s or P_a ($P_a = P_1 + P_2$) represent the mobile robot's power consumption for straight or curved paths, depending on the wheels' angular speed and acceleration ($\dot{\theta}_1(t)$, $\ddot{\theta}_1(t)$) for an interval time $t_0 < t < t_f$ between an initial (t_0) and final (t_f) time, considering a not fixed t_f. On the other hand, the angular speed ($\dot{\theta}_1(t)$), at the moment of following a straight or curved path by the robot is delimited by the initial (v_0) and final (v_f) speeds of the wheel subject to $v_0 < v_m$, $v_f < v_m$, where v_m is the maximum speed of the wheel. In this case, the optimal problem to solve considers the angular speed $\dot{\theta}_1$ of the wheel with fixed initial (v_0) and final (v_f) conditions and a free t_f.

2.2.2 Necessary Conditions for Optimal Control

The optimal problem to solve is related to determining an admissible u^* control variable and the necessary optimal conditions that cause the system to follow an admissible trajectory x^* that minimizes the performance measure [3]

$$\dot{x} = \mathbf{a}(x(t), u(t), t)\,. \tag{35}$$

Notice that there are necessary conditions to determine related to equation (35). The necessary conditions consist of a set of first-order differential equations (the state and costate equations) and a set of algebraic relations which must be satisfied throughout the interval [t_0,t_f]. The solution of the state and costate equations will contain constants of integration. A set of equations $x^*(t_o) = x_0$ and $x^*(t_f) = x_f$ related to boundary conditions are used to evaluate these constants [3]. In the following, to solve the problem, it is convenient to use the function H, called the Hamiltonian, defined by [1, 3, 26]:

$$H(x(t), u(t), \lambda(t), t) = \mathbf{f}(x(t), u(t), \lambda(t), t) + \lambda(t)\mathbf{g}(x(t), u(t), t)\,. \tag{36}$$

In our case, the power model P (depending on the analysis, is either P_s or P_a) is the cost function to optimize (**f**), x is the state variable vector, and λ = [λ_1(t) $\lambda_2(t)$] are the auxiliary variables called Lagrange multipliers that allow to introduce the control variable a_{θ_1} (u^* = a_{θ_1}) where v_{θ_1} = $\dot{\theta}_1$, a_{θ_1} = $\ddot{\theta}_1$, and **g** = $[v_{\theta_1}(t)\ a_{\theta_1}(t)]^T$ (The Lagrange multipliers in this section are not related with the simplified Lagrange multipliers used in the power model mathematical procedure early). Then, the Hamiltonian function to solve the specific optimal problem to obtain an admissible trajectory $a^*(t)$ that minimizes the power consumption value of the robot for a straight or curved path is defined by

$$H(x, a_{\theta_1}, \lambda, t) = P(v_{\theta_1}, a_{\theta_1}, t) + \lambda_1(t)v_{\theta_1} + \lambda_2(t)a_{\theta_1}\,. \tag{37}$$

The necessary condition for $a^*_{\theta_1}(t)$ to optimize the Hamiltonian function for all time [t_0 t_f] are given by

$$\dot{\theta_1} = \frac{\partial H}{\partial \lambda_1}\,, \qquad \dot{\lambda_1} = -\frac{\partial H}{\partial \theta_1}\,, \qquad 0 = \frac{\partial H}{\partial a_{\theta_1}}\,,$$
$$\dot{v}_{\theta_1} = \frac{\partial H}{\partial \lambda_2}\,, \qquad \dot{\lambda_2} = -\frac{\partial H}{\partial v_{\theta_1}}\,.$$

Some partial derivatives of the necessary optimal condition are easy to verify, considering that the power model (P) does not depend on the Lagrange multipliers or the angular position of the wheels:

$$\frac{\partial H}{\partial \lambda_1} = v_{\theta_1}\,, \qquad \frac{\partial H}{\partial \lambda_2} = a_{\theta_1}\,, \qquad -\frac{\partial H}{\partial \theta_1} = 0\,.$$

The results of these optimal conditions are congruent ($v_{\theta_1} = \dot{\theta_1}$, $a_{\theta_1} = \dot{v_{\theta_1}}$), which do not help to obtain an expression for $a^*(t)$. On the other hand, the results from the remaining optimal conditions give

$$\frac{\partial H}{\partial a_{\theta_1}} = \lambda_2 + s(v_{\theta_1}, a_{\theta_1}, t)\,, \qquad \frac{\partial H}{\partial v_{\theta_1}} = -\lambda_1 - t(v_{\theta_1}, a_{\theta_1}, t)\,.$$

The functions s and t represent large nonlinear equations depending on variables states and dynamic parameters of the robot and motors. Matching the partial derivative results with the necessary optimal condition presented earlier gives the following equations:

$$0 = \lambda_2 + s(v_{\theta_1}, a_{\theta_1}, t)\,, \qquad \dot{\lambda_2} = -\lambda_1 - t(v_{\theta_1}, a_{\theta_1}, t)\,.$$

Isolating λ_2 from the left expression and applying derivative with respect to time on both sides gives $\dot{\lambda_2} = -\dot{s}(v_{\theta_1}, a_{\theta_1}, t)$. Finally, matching both expressions of $\dot{\lambda_2}$, the following is obtained:

$$\dot{s}(v_{\theta_1}, a_{\theta_1}, t) = \lambda_1 + t(v_{\theta_1}, a_{\theta_1}, t)\,. \tag{38}$$

After taking the derivatives, simplifying the terms, and reordering equation (38), the following nonlinear differential equation, which does not depend on λ_2, is obtained:

$$0 = \mathrm{c}_1\, \ddot{\mathrm{v}}_{\theta_1} - \mathrm{c}_2\, \mathrm{v}_{\theta_1} - \frac{\mathrm{c}_3 + \lambda_1}{2}\,. \tag{39}$$

In the case of the straight path, the parameters c_1, c_2 and c_3 are obtained as

$$c_1 = \frac{R {I_e}^2}{2 {K_t}^2 n^2}\,, \tag{40}$$
$$c_2 = \frac{2\,\nu\,\left(K_t\,K_v\,n^2 + R\,\nu\right)}{{K_t}^2\,n^2}\,, \tag{41}$$
$$c_3 = \frac{2\,T_m\,\left(K_t\,K_v\,n^2 + 2\,R\,\nu\right)}{{K_t}^2\,n^2}\,. \tag{42}$$

For the curved path, taking into account the power consumption of both motors, the parameters are

$$c_1 = \frac{R\left((aI_e - I_p)^2 + (I_e + I_p)^2\right)}{4K_t^2 n^2}\,, \tag{43}$$

$$c_2 = \frac{\nu\big(a^2+1\big)\big(K_t K_v n^2 + R\nu\big)}{K_t^2 n^2}\,, \tag{44}$$

$$c_3 = \frac{T_m\big(K_t K_v n^2 + 2R\nu\big)(\|a\|+1)}{K_t^2 n^2}\,. \tag{45}$$

Note that c_1, c_2, and c_3 look different for the optimum speed profiles of the straight and the curved paths (all the mathematical procedures in this section were developed in Matlab using the functions diff, simplify, and collect). However, they converge to the same value as a tends to 1. The solution of the differential equation (39), which minimizes the robot's energy consumption when it moves in a straight or curved path, is

$$v^*_{\theta_1} = s_1 e^{tk} + s_2 e^{-tk} + s_3\,, \tag{46}$$

where

$$s_3 = -\frac{c_3 + \lambda_1}{2c_2}\,, \tag{47}$$

$$k = \sqrt{\frac{c_2}{c_1}}\,. \tag{48}$$

The optimal acceleration and pose of the wheels are calculated using the derivative and integral of the optimal speed, and they are respectively given as

$$a^*_{\theta_1}(t) = s_1 k e^{kt} - s_2 k e^{-kt}\,, \tag{49}$$

$$\theta^*_1(t) = \frac{s_1}{k} e^{kt} - \frac{s_2}{k} e^{-kt} + s_3 t + s_4\,. \tag{50}$$

These variables are important to calculate the unknown parameters of equation (46).

2.2.3 Optimization Constraint Parameters

The initial and final conditions of the wheel's speed and pose are used to calculate the unknown parameters of the optimal speed of the wheels s_1, s_2, s_3, s_4 and λ_1. The boundary conditions, delimited by the problem statement, are given as follows:

$$\theta_1(0) = 0\,,\;\; v_{\theta_1}(0) = v_o\,,\;\; \theta_1(t_f) = \theta_f\,,\;\; v_{\theta_1}(t_f) = v_f\,, \tag{51}$$

where θ_f is the total angular position of the wheel when the robot moves forward in a straight or curved path. Once the conditions are evaluated in equations (46) and (50), the following nonlinear system of equations is obtained:

$$\begin{aligned}
\frac{s_1}{k} - \frac{s_2}{k} + s_4 &= 0\,,\\
s_1 + s_2 + s_3 &= v_o\,,\\
\frac{s_1}{k}e^{kt_f} - \frac{s_2}{k}e^{-kt_f} + s_3 t_f + s_4 &= \theta_f\,,\\
s_1\, e^{kt_f} + s_2\, e^{-kt_f} + s_3 &= v_f\,.
\end{aligned} \tag{52}$$

The solution to the above nonlinear system of equations gives the unknown parameters of the optimal speed of the wheels in terms of the final time t_f as

$$s_1 = \frac{(v_0 - v_f - k\theta_f + kt_f v_f)\, e^{kt_f} + v_f - v_0 + k\theta_f - kt_f v_0}{4e^{kt_f} + (kt_f - 2)\, e^{2kt_f} - kt_f - 2}\,, \tag{53}$$

$$s_2 = \frac{(v_0 - v_f + k\theta_f - kt_f v_f)\, e^{kt_f} + (v_f - v_0 - k\theta_f + kt_f v_0)\, e^{2kt_f}}{4e^{kt_f} + (kt_f - 2)\, e^{2kt_f} - kt_f - 2}\,, \tag{54}$$

$$s_3 = \frac{(k\theta_f - v_f - v_0)\, e^{kt_f} + v_0 + v_f + k\theta_f}{(kt_f - 2)\, e^{kt_f} + kt_f + 2}\,. \tag{55}$$

λ_1 and λ_2 are found respectively as

$$\lambda_1 = -2s_3c_2 - c_3\,, \tag{56}$$

$$\begin{aligned}
\lambda_2 = &-2c_1 - \frac{\left(K_t K_v n^2 + 2R\nu\right)\left(I_e + I_p - a\,(I_p - aI_e)\right)}{2K_t^2 n^2} v_{\theta_1}\\
&+ \frac{RT_m\left(I_p\,(\operatorname{sgn} a - 1) - I_e\,(1 + \|a\|)\right)}{K_t^2 n^2}\,.
\end{aligned} \tag{57}$$

2.2.4 Final Time of the Optimal Speed Profile

Considering the problem statement, the optimal problem has a horizontal line, which means a fixed terminal, an "endpoint" for the state variables ($v_{\theta_1}(t_f) = v_f$, and $\theta_1(t_f) = \theta_f$), with a free terminal time (t_f). Therefore, the transversality condition for this case, to calculate the final time t_f is [1]

$$H(a_{\theta_1}(t_f), v_{\theta_1}(t_f), \lambda_1(t_f), \lambda_2(t_f)) = 0\,. \tag{58}$$

In the case of the straight path, the transversality condition is given by

$$P_s(a_{\theta_1}(t_f), v_{\theta_1}(t_f)) + \lambda_1(t_f) v_{\theta_1}(t_f) + \lambda_2(t_f) a_{\theta_1}(t_f) = 0\,,$$

and for the curved path, the transversality condition is given by

$$P_a(a_{\theta_1}(t_f), v_{\theta_1}(t_f)) + \lambda_1(t_f) v_{\theta_1}(t_f) + \lambda_2(t_f) a_{\theta_1}(t_f) = 0\,.$$

Figure 2: The Nomad Super Scout used in the experiments. The picture shows the robot with the payload

3 Experimental Setup

The experiments in this work were performed using a Nomad Super Scout II, a commercial two wheel differential drive mobile robot (Fig. 2). The robot wheel speeds are controlled by a built-in Motorola 68332 embedded controller, which receives speed commands over a serial port, and then controls the motor drivers accordingly. The board also reads the encoders and sends back the information. In order to measure motor voltages and currents in real time, a custom power monitor was built, sampling motor terminals at $500\,\mathrm{Hz}$ through an analog-to-digital converter (SMT32F103C8). Both the embedded robot controller and the custom power monitor were connected to an Orange-Pi PC Plus single-board computer running Armbian and Robot Operating System (ROS). The computer was used for high-level control of the robot, i.e., to set speeds and accelerations and to record power and encoder data for later offline analysis. The robot weighs $23.6\,\mathrm{kg}$, and an external $10.8\,\mathrm{kg}$ payload was used in some of the tests. The half-basewidth and the wheel radius of the robot are $0.165\,\mathrm{m}$, and $0.1\,\mathrm{m}$, respectively. The size variables and motor constants were taken from the data sheet, whereas the friction torques required by the power model were found by a calibration, running the robot along straight line segments and estimating the friction values using least squares. A more detailed description of the procedure can be found in [14].

4 Experimental Results and Discussions

In order to validate and assess performance improvements of the optimal speed profiles generated using the method described in this paper, the Nomad Super Scout II was driven in straight line segments and curves of various radii of curvature, on a polished stone surface, both with and without payload. In this procedure, various trapezoidal and optimal speed profiles were utilized (Fig. 3). Trapezoidal speed profiles were employed as baseline for comparison due to the fact that they are de facto speed profiles used in robots, and each robot usually have a default one preprogrammed with a default acceleration, which may also be the only option available on the robot. This profile is easily performed by the controllers just by setting a target speed. The trapezoidal speed profile is also the easiest for a user that is not worried about energy efficiency.

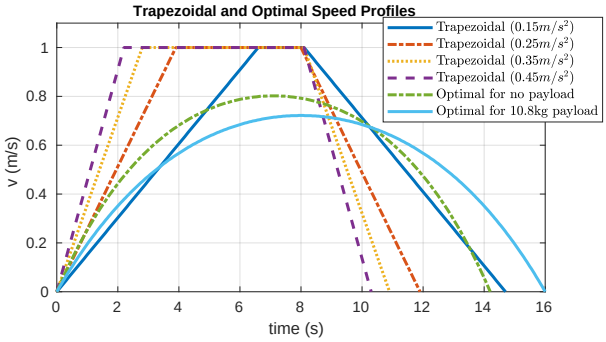

Figure 3: Different speed profiles used in the tests for the 8 m long trajectory.

As shown in this work, an optimal speed profile requires significantly extra information about the robot, such as motor parameters, weight of the platform, and even friction of the surface, which would require a calibration procedure if not known beforehand.

4.1 Straight Path Tests

For tests along straight paths, the speed was constrained to a maximum of 1 m/s, but the accelerations were varied from $0.15\,\text{m/s}^2$ up to $0.45\,\text{m/s}^2$, the default acceleration of the robot controller. The robot was commanded to cover distances of 1 m, 2 m, 4 m, and 8 m using the different speed profiles. To alleviate small variations in power consumption due to surface irregularities, each run was repeated 5 times.

Experimental measurements of the consumed energy without a payload and with a 10.8 kg payload are presented on Tables 2 and 3. These tables show that the power consumption of the robot is increasing with increasing accelerations for the trapezoidal speed profiles. As expected, it can also be seen that the optimal speed profiles consume less energy than the trapezoidal profiles in almost all the cases. Fig. 4 shows the energy savings for different speed profiles compared with the default. The percentage energy savings are calculated using

$$\text{saving}(\%) = \frac{\text{E}(\text{DefaultTrap.}) - \text{E}(\text{Profile})}{\text{E}(\text{DefaultTrap.})} \times 100\,. \tag{59}$$

The default trapezoidal profile, which is also the speed profile used by the robot controller, has an acceleration of $0.45\,\text{m/s}^2$. In comparison to this profile, decreasing the accelerations and decelerations saves energy. However, all are outperformed by the optimal speed profile developed in this work. The optimal speed profile leads to savings of 28% with no payload, and 35% with payload. Compared to the best trapezoidal profile, which has an acceleration of $0.15\,\text{m/s}^2$, savings are still significant, especially when the robot is carrying a payload. With a payload, the optimal profiles save 7.5% more along the 4 m long trajectory, and 5% more along shorter trajectories. However, at 8 m long paths, the savings are moderate compared with the best trapezoidal profile, staying around 3%, though the overall savings reach 20%. With longer trajectories the

Table 2: Energy consumption of the robot with no payload using different speed profiles along different lines

	Energy Consumed (J)			
Speed Profile	For 1 m	For 2 m	For 4 m	For 8 m
Trap. ($0.15\,\mathrm{m/s^2}$)	11.60	20.56	38.35	74.73
Trap. ($0.25\,\mathrm{m/s^2}$)	12.06	22.03	42.40	76.43
Trap. ($0.35\,\mathrm{m/s^2}$)	13.26	25.16	44.49	80.04
Trap. ($0.45\,\mathrm{m/s^2}$)	15.05	27.55	45.34	78.71
Optimal	11.41	19.75	38.48	72.79

Table 3: Energy consumption of the robot with 10.8 kg payload using different speed profiles along different lines

	Energy Consumed (J)			
Speed Profile	For 1 m	For 2 m	For 4 m	For 8 m
Trap. ($0.15\,\mathrm{m/s^2}$)	15.72	28.08	50.86	95.49
Trap. ($0.25\,\mathrm{m/s^2}$)	17.20	31.96	57.79	99.93
Trap. ($0.35\,\mathrm{m/s^2}$)	20.21	37.51	63.44	106.23
Trap. ($0.45\,\mathrm{m/s^2}$)	22.12	40.06	61.88	105.31
Optimal	14.53	25.84	46.19	92.48

optimal profile and the trapezoidal profile are expected to eventually converge, differing only in the initial and final accelerations and decelerations, and hence value-wise, the difference is expected to be small and the ratio is expected to decrease, as is confirmed by the relatively small 3% improvements for 8 m. During routine operation, the shortest and most energy-saving paths are straight line segments connecting the start and end positions. However, obstacles force the robots to divide long trajectories into smaller parts. This forces the robot to drive at different speeds along the path, changing between different line segments at times with smooth rotations, at times with full stop and start. Using optimal velocity profiles along these smaller segments will lead to considerable cumulative energy savings for the robot. Another advantage of the optimal speed profiles is the lower maximum speeds (Fig. 3), which allow the robot to stop earlier in case of unexpected dynamic obstacles.

4.2 Rotational Tests

In order to measure performance along curves, the robot was commanded to perform rotations of 90^{o}, imitating a robot that is changing corridors. The radius of curvature was varied from 0.5 m to 2 m, and the accelerations were varied from 0.05 to 0.45 m/s. However, the accelerations were set for the outer, i.e. the faster wheel, due to the

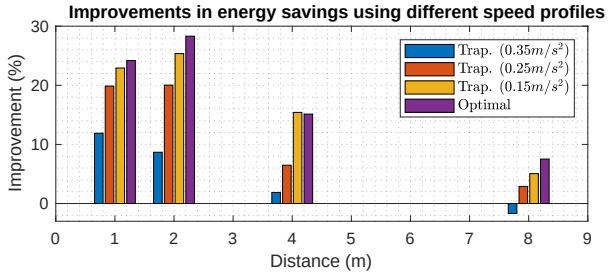

(a)

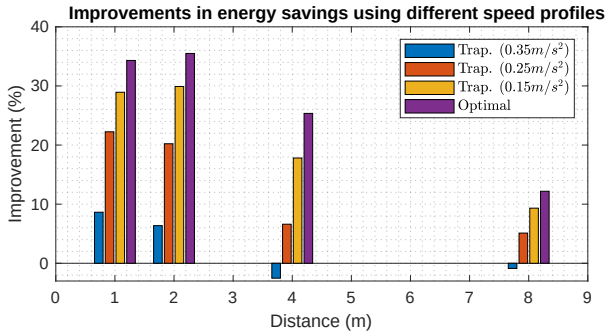

(b)

Figure 4: Energy savings (in %) along different paths compared with the default speed profile (a) with no payload, (b) with 10.8 kg payload.

configured acceleration limit of the robot. The measured consumption values are presented on Tables 4 and 5, and the corresponding savings, which were calculated using equation (59), are presented in Fig. 5. Energy consumptions presented on the tables increase with increasing accelerations. Almost all consumption values exceed the optimum. Consumption is also increasing with increasing radius of curvature, which is expected as larger radii of curvature correspond to longer covered distances. As can be seen from Table 6, where the durations of trajectories with different accelerations are given, despite consuming minimum energy, optimum speed profiles are not the quickest, and excluding the $0.05\,\text{m/s}^2$ acceleration, they take the longest. For a radius of curvature of $2\,\text{m}$, the optimal profile takes $10.7\,\text{s}$, which is almost twice the duration of the fastest trapezoidal speed profile, which has $0.45\,\text{m/s}^2$ acceleration. However, the energy consumption is almost 18% better.

4.3 Effects of Payload on the Optimal Speed Profile

In this subsection, we analyze how the payload changes the optimal speed profiles. For this, assuming a radius of curvature of $2\,\text{m}$ and an arc of 90^o, the Hamiltonian formalism was solved for a series of payloads varying from $0\,\text{kg}$ to $60\,\text{kg}$, and the corresponding optimum speed profiles were obtained. Then for each optimum profile, the

Table 4: Energy consumption of the robot with no payload using different speed profiles along different arcs (90^{o})

	Energy Consumed (J)			
Spd. Profile	0.5 m	1 m	1.5 m	2 m
Trap. ($0.05\,\mathrm{m/s^2}$)	11.50	19.68	27.70	34.87
Trap. ($0.15\,\mathrm{m/s^2}$)	10.29	18.02	25.71	33.76
Trap. ($0.25\,\mathrm{m/s^2}$)	9.65	17.33	25.56	33.40
Trap. ($0.35\,\mathrm{m/s^2}$)	10.21	18.94	28.83	34.98
Trap. ($0.45\,\mathrm{m/s^2}$)	10.98	21.55	29.24	37.02
Optimal	9.15	16.71	24.47	32.56

Table 5: Energy consumption of the robot with 10.8 kg payload using different speed profiles along different arcs (90^{o})

	Energy Consumed (J)			
Spd. Profile	0.5 m	1 m	1.5 m	2 m
Trap. ($0.05\,\mathrm{m/s^2}$)	14.87	25.56	34.58	43.26
Trap. ($0.15\,\mathrm{m/s^2}$)	13.29	24.49	33.27	41.25
Trap. ($0.25\,\mathrm{m/s^2}$)	13.25	23.31	32.54	43.85
Trap. ($0.35\,\mathrm{m/s^2}$)	14.23	27.37	38.87	46.57
Trap. ($0.45\,\mathrm{m/s^2}$)	15.81	30.39	41.58	49.11
Optimal	12.09	22.06	31.38	40.63

Table 6: Duration of different speed profiles along 90^{o}circular paths with 10.8 kg payload.

	Duration (s)			
Spd. Profile	0.5 m	1.0 m	1.5 m	2.0 m
Trap. ($0.05\,\mathrm{m/s^2}$)	9.2	12.1	14.5	16.4
Trap. ($0.15\,\mathrm{m/s^2}$)	5.2	7.0	8.3	9.6
Trap. ($0.25\,\mathrm{m/s^2}$)	4.0	5.5	6.5	7.4
Trap. ($0.35\,\mathrm{m/s^2}$)	3.5	4.5	5.5	6.3
Trap. ($0.45\,\mathrm{m/s^2}$)	3.1	4.0	4.9	5.7
Optimal	5.2	7.4	9.2	10.7

maximum speed and the duration of the profile were calculated, plotting the results in Fig. 6. As can clearly be seen in the figure, increasing the payload decreases the maximum speed, which consequently increased the mission time. The changes, however,

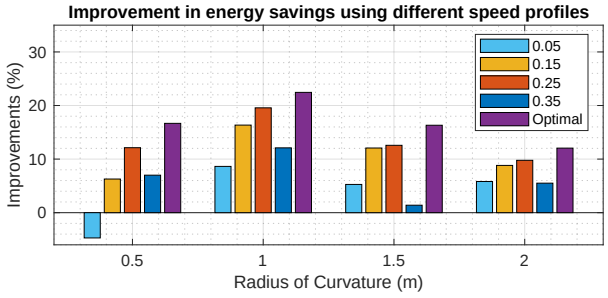

(a)

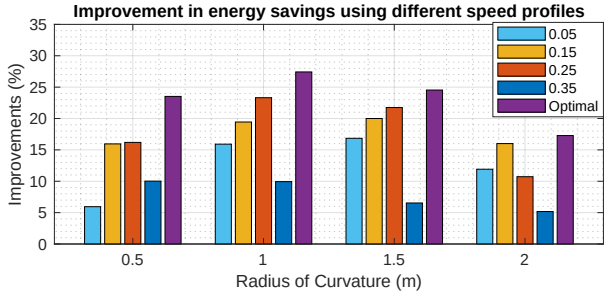

(b)

Figure 5: Energy savings (in %) along curves with different radius of curvatures compared with the default speed profile (a) with no payload, (b) with 10.8 kg payload.

were not linear. A 90^{o} turn took 9.3 s with no payload, with a corresponding maximum translational speed of 0.5 m/s. Increasing the payload to 10 kg and 20 kg increased the mission durations by 1.3 s and 2.5 s respectively, whereas the maximum linear speeds decreased down to 0.44 m/s and 0.39 m/s respectively. These changes are expected, as with increasing mass, the energy needed to speed up the robot also increases. And the only way for the optimum profiles to keep competitive, is to reduce the maximum speed, which in turn increases profile durations.

5 Conclusion

Energy minimization is a current and important problem, that is studied across a wide range of disciplines. The energy minimization problem in robotics, particularly regarding wheeled mobile robots, has been approached from different angles, such as improving utilization, planning shorter paths, and improving speed trajectories, among others. In this context, this work focused on improving speed trajectories of two wheel differential drive robots, presenting a set of energy optimal speed profiles for straight and curved paths. In order to find the speed profiles, a recently published robot power model that explicitly contains all motor and robot parameters as well as friction and payload was used in a Hamiltonian formalism. The resulting speed profiles were found

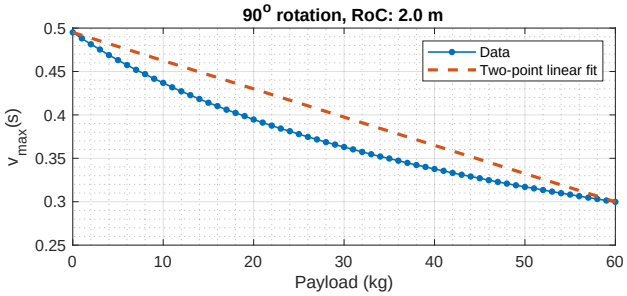

(a)

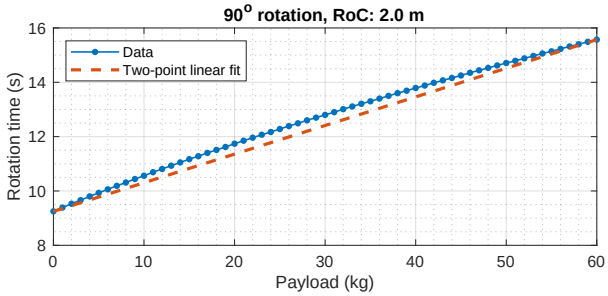

(b)

Figure 6: Variations in maximum linear speed of the optimum speed profile (a) and its durations (b) as the payload is increased from 0 kg to 60 kg.

to be the sum of two exponential terms and an offset. The coefficients and the exponents were calculated using the boundary conditions and zero crossing of the Hamiltonian. The resulting speed profiles, which were found both for straight and curved paths, were experimentally validated using a commercial mobile robot, namely the Nomad Super Scout II. The energy consumptions of the profiles were compared with the energy consumptions of the trapezoidal speed profiles, and considerable savings in energy consumption were observed. The savings were positively correlated with payload, which means the heavier the robot or the load it carries, the more it benefits from optimization. Relative savings were observed to be more significant along shorter path segments. This is because as the path gets longer, the relative contributions of the start and end of the path, where the accelerations are observed, to the consumed energy become smaller. However, the savings were experimentally observed to be still important up to at least 8 m. For rotational trajectories, savings were also significant, particularly compared with the default trapezoidal speed profile. The proposed optimum speed profiles, containing all relevant motor and robot parameters explicitly, allow easy adaptation to different differential drive platforms with minimal efforts.

Acknowledgements

This work was supported by AM2R project "Mobilizing Agenda for business innovation in the Two Wheels sector" funded by PRR - Recovery and Resilience Plan and by the Next Generation EU Fund, under reference C644866475-00000012 | 7253; and HAVATAR project funded by FCT - Fundação para a Ciência e a Tecnologia, under reference PTDC/EEI-ROB/1155/2020.

References

[1] Alpha C Chiang. Elements of dynamic optimization. McGraw-Hill, 1992.

[2] Hamidreza Chitsaz, Steven M. LaValle, Devin J. Balkcom, and Matthew T. Mason. Minimum wheel-rotation paths for differential-drive mobile robots. The International Journal of Robotics Research, 28(1):66–80, 2009.

[3] Kirk DE. Optimal Control Theory : An Introduction. Prentice-Hall, 1970.

[4] S. Dogru and L. Marques. A physics-based power model for skid-steered wheeled mobile robots. IEEE Transactions on Robotics, 34(2):421–433, 2018.

[5] Sedat Dogru and Lino Marques. Improved coverage path planning using a virtual sensor footprint: a case study on demining. In 2019 International Conference on Robotics and Automation (ICRA), pages 4410–4415, 2019.

[6] Lester E Dubins. On curves of minimal length with a constraint on average curvature, and with prescribed initial and terminal positions and tangents. American Journal of Mathematics, 79(3):497–516, 1957.

[7] Thierry Fraichard and Alexis Scheuer. From reeds and shepp's to continuous-curvature paths. IEEE Transactions on Robotics, 20(6):1025–1035, 2004.

[8] Andrei A. Furtuna and Devin J. Balkcom. Generalizing dubins curves: Minimum-time sequences of body-fixed rotations and translations in the plane. The International Journal of Robotics Research, 29(6):703–726, 2010.

[9] Nuwan Ganganath, Chi-Tsun Cheng, and Chi K. Tse. A constraint-aware heuristic path planner for finding energy-efficient paths on uneven terrains. IEEE Transactions on Industrial Informatics, 11(3):601–611, 2015.

[10] A. Gholipour and M. J. Yazdanpanah. Dynamic tracking control of nonholonomic mobile robot with model reference adaptation for uncertain parameters. In 2003 European Control Conference (ECC), pages 3118–3122, 2003.

[11] Veronica Gruning, Jesse Pentzer, Sean Brennan, and Karl Reichard. Energy-aware path planning for skid-steer robots operating on hilly terrain. In 2020 American Control Conference (ACC), pages 2094–2099, 2020.

[12] Nikhil Gupta, Camilo Ordonez, and Emmanuel Collins. Dynamically feasible, energy efficient motion planning for skid-steered vehicles. Autonomous Robots, 41:453–471, 2 2017.

[13] D. Ho, K. Ben Chehida, B. Miramond, and M. Auguin. Towards a multi-mission qos and energy manager for autonomous mobile robots. In 2018 Second IEEE International Conference on Robotic Computing (IRC), pages 270–273, 2018.

[14] Mauricio F. Jaramillo-Morales, Sedat Dogru, Juan Bernardo Gómez-Mendoza, and Lino Marques. Energy estimation for differential drive mobile robots on straight and rotational trajectories. International Journal of Advanced Robotic Systems, 17(2):1729881420909654, 2020.

[15] Mauricio F. Jaramillo-Morales, Sedat Dogru, and Lino Marques. Generation of energy optimal speed profiles for a differential drive mobile robot with payload on straight trajectories. In 2020 IEEE International Symposium on Safety, Security, and Rescue Robotics (SSRR), pages 136–141, 2020.

[16] Chong Hui Kim and Byung Kook Kim. Minimum-energy motion planning for differential-driven wheeled mobile robots. In Xing-Jian Jing, editor, Motion Planning, chapter 11. IntechOpen, Rijeka, 2008.

[17] Shuang Liu and Dong Sun. Minimizing energy consumption of wheeled mobile robots via optimal motion planning. IEEE/ASME Transactions on Mechatronics, 19(2):401–411, 2014.

[18] Daniel Léonard and Ngo van Long. Optimal Control Theory and Static Optimization in Economics. Cambridge University Press, 1992.

[19] Yongguo Mei, Yung-Hsiang Lu, Y.C. Hu, and C.S.G. Lee. Energy-efficient motion planning for mobile robots. In IEEE International Conference on Robotics and Automation, 2004. Proceedings. ICRA '04. 2004, volume 5, pages 4344–4349 Vol.5, 2004.

[20] J. Morales, J. L. Martinez, A. Mandow, A. J. Garcia-Cerezo, and S. Pedraza. Power consumption modeling of skid-steer tracked mobile robots on rigid terrain. IEEE Transactions on Robotics, 25(5):1098–1108, 2009.

[21] R. Parasuraman, K. Kershaw, P. Pagala, and M. Ferre. Model based on-line energy prediction system for semi-autonomous mobile robots. In 2014 5th International Conference on Intelligent Systems, Modelling and Simulation, pages 411–416, 2014.

[22] James Reeds and Lawrence Shepp. Optimal paths for a car that goes both forwards and backwards. Pacific Journal of Mathematics, 145(2):367–393, 1990.

[23] V. Sathiya and M. Chinnadurai. Evolutionary algorithms-based multi-objective optimal mobile robot trajectory planning. Robotica, 37(8):1363–1382, 2019.

[24] Werther Serralheiro, Newton Maruyama, and Fabrício Saggin. Self-Tuning Time-Energy Optimization for the Trajectory Planning of a Wheeled Mobile Robot. Journal of Intelligent & Robotic Systems, 95(3):987–997, September 2019.

[25] Omar Serrano-Pérez, Miguel G. Villarreal-Cervantes, Juan C. González-Robles, and Alejandro Rodríguez-Molina. Meta-heuristic algorithms for the control tuning of omnidirectional mobile robots. Engineering Optimization, 52(2):325–342, 2020.

[26] Pratap Tokekar, Nikhil Karnad, and Volkan Isler. Energy-optimal trajectory planning for car-like robots. Autonomous Robots, 37:279–300, 10 2014.

[27] Li Xie, Christian Henkel, Karl Stol, and Weiliang Xu. Power-minimization and energy-reduction autonomous navigation of an omnidirectional mecanum robot via the dynamic window approach local trajectory planning. International Journal of Advanced Robotic Systems, 15(1):1729881418754563, 2018.

[28] Y. Yamamoto and Xiaoping Yun. Coordinating locomotion and manipulation of a mobile manipulator. IEEE Transactions on Automatic Control, 39(6):1326–1332, 1994.

[29] X. Yun and Y. Yamamoto. Internal dynamics of a wheeled mobile robot. In Proceedings of 1993 IEEE/RSJ International Conference on Intelligent Robots and Systems (IROS '93), volume 2, pages 1288–1294 vol.2, 1993.